17th World Conference on Earthquake Engineering, 17WCEE
Sendai, Japan - September 13th to 18th 2020

SHEAR BRIDGING CHARACTERISTICS OF ARAMID AND PP FIBERS ON CRACK SURFACE OF FRCC

S. Asayama[(1)], A. Yasojima[(2)]

[(1)] *Graduate Student, Dept. of Engineering Mechanics and Energy, University of Tsukuba, Japan, s1920879@s.tsukuba.ac.jp*
[(2)] *Associate Professor, Dept. of Engineering Mechanics and Energy, University of Tsukuba, Japan, yasojima@kz.tsukuba.ac.jp*

Abstract

Fiber Reinforced Cementitious Composite (FRCC), in which short fibers of several percentage of volume fraction are mixed with mortar or concrete, shows the improved tensile and bending characteristics of cementitious composites elements. FRCC is expected to be applied to structural members with high performance in ductility, because short fibers bridge the crack after first cracking and transfer the tensile force. In order to design damage-controlled structural members with FRCC, it is important to elucidate the shear bridging characteristics of the fibers in FRCC on the shear crack surface.

In this study, single plane shear tests under tensile load as normal stress on a crack surface are conducted to clarify the shear transfer mechanism of aramid fibers and polypropylene (PP) fibers on multiple stress condition of FRCC members. Specimens have an assumed crack surface at which aramid or PP fibers are embedded in a constant interval. Experimental factors are the tensile force on fibers bridging cracks, the fiber type and orientation angle of embedded fibers.

From the test results, the shear stiffness on the crack surface with fibers under tensile stress was confirmed to change depending on the fiber type and the orientation angle of fibers. In the case of the lower tensile force applied to fibers on the crack surface, the shear strength of aramid and PP fiber decreased linearly with increasing the tensile force. The maximum shear stress of both fibers under biaxial stress state was about one-third of uniaxial tensile strength calculated by the bridging law despite the difference of the fiber type and the orientation angle of fibers.

Keywords: FRCC; biaxial stress; bridging law; aramid fiber; polypropylene fiber

1. Introduction

Fiber Reinforced Cementitious Composite (FRCC) is cementitious material reinforced by short discrete fibers of several percentage in volume fraction which are mixed with mortar or concrete. FRCC shows the improved tensile and bending characteristics of cementitious composites by bridging effect of short fibers through the crack. By applying FRCC to structural members, it is expected to improve structural performance and inhibit crack damage. However, it is difficult to evaluate fiber bridging effect in FRCC. Fiber bridging characteristics are depend on the fiber type, the fiber orientation and distribution in matrix. In order to establish the evaluation method of FRCC members, it is important to elucidate the shear bridging characteristics of various fibers on the shear crack surface of FRCC members.

The objective of this study is to investigate the shear bridging characteristics of aramid fibers and polypropylene (PP) fibers on shear crack surface of FRCC structural members. Single plane shear tests under tensile load as normal stress on a crack surface are carried out for specimens that have an assumed crack surface with embedded aramid or PP fibers. Based on the experimental results, shear bridging characteristics of aramid and PP fibers under biaxial stress and the effect of fiber type and orientation angle are considered.

2. Experimental Program

2.1 Test specimens

The appearance and mechanical properties of fibers used in this study are shown in Fig. 1 and Table 1. Aramid fiber has been stranded from single fine fibers. The surface of the PP fiber has embossed to improve the bond property. Aramid fiber and PP fiber are fibrillated with a same length of 30mm. Diameter for aramid and PP fiber is 0.5mm and 0.7mm independently. Aramid fibers having an extraordinary tensile strength of 3432 MPa have been used in aircraft, military vehicles, bullet proof vests and many other.

Fig. 2 shows the dimension of the specimens for single plane shear test under tensile stress. The examples of partition plate with embedded fibers are also shown in Fig. 2. The specimen is a prism of 70mm × 100mm × 400mm. The notches are set at the central position of specimen and the sectional size of shear plane is 70mm × 70mm. The 3mm thick partition plate is installed on the assumed crack surface with embedded aramid or PP fibers. A total number of 196 aramid or PP fibers is embedded in the partition plate at 5mm intervals. The parameters are fiber type, the orientation angle of embedded fiber, the constant tensile force on the crack surface with embedded fibers. The identification of specimen is shown in Fig. 3.

The definition of fiber orientation angle θ_{xy} is shown in Fig. 4. The three types of fiber orientation angle in specimen were prepared: 196 fibers with θ_{xy} = 0° embedded, 196 fibers with θ_{xy} = 30° embedded, 98 fibers with θ_{xy} = 0°and 98 fibers with θ_{xy} = 30° embedded (hereinafter called θ_{xy} = (0°, 30°)). The embedded length of fiber on one side is adjusted to be 12mm at any orientation angle. The M16 screw bolts were embedded at the both ends of specimen to apply tensile force to the crack surface with embedded fibers. The number of specimens for aramid and PP fiber is 3 and 4 for each orientation angle, respectively. Polyvinyl alcohol (PVA) fibers (length 12mm, diameter 0.1mm, tensile strength 1200MPa) were mixed into the FRCC matrix of specimen with a fiber volume fraction of 0.5% to prevent cracks doe to drying shrinkage and tensile force.

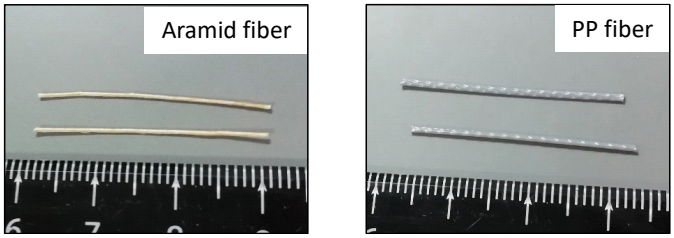

Fig. 1 –Appearance of embedded fiber

Table 1 – Mechanical properties of fiber

Fiber type	Length (mm)	Diameter (mm)	Tensile strength (MPa)	Elastic modulus (GPa)
Aramid	30	0.5	3,432	73
PP	30	0.7	580	4.9

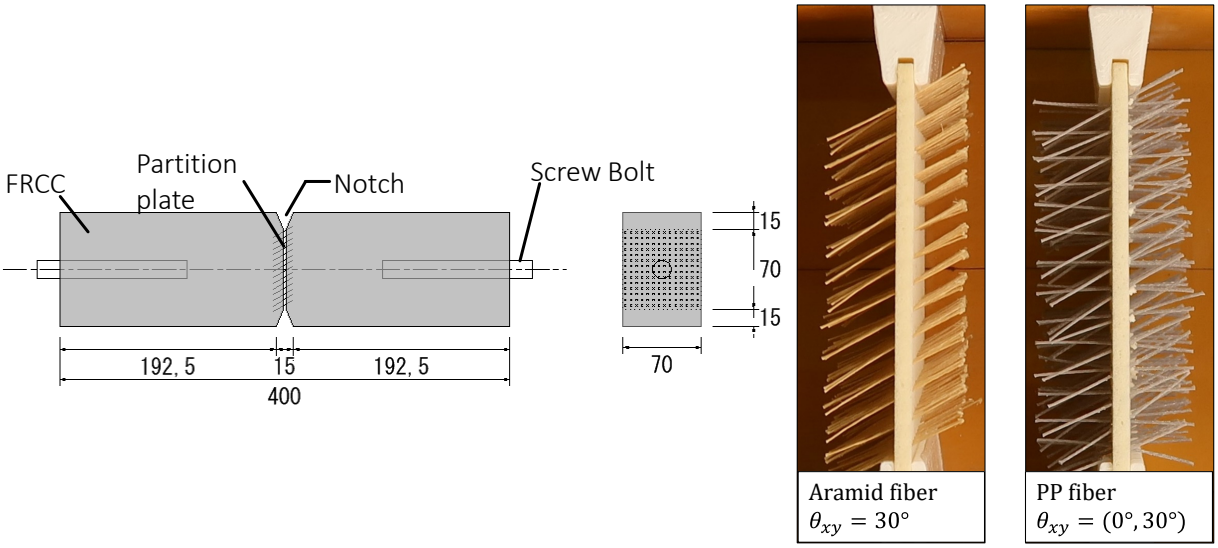

Fig. 2 – Specimen dimensions and examples of partition plate

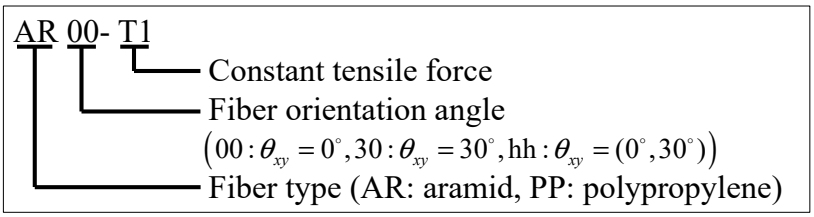

Fig. 3 – Identification of specimen

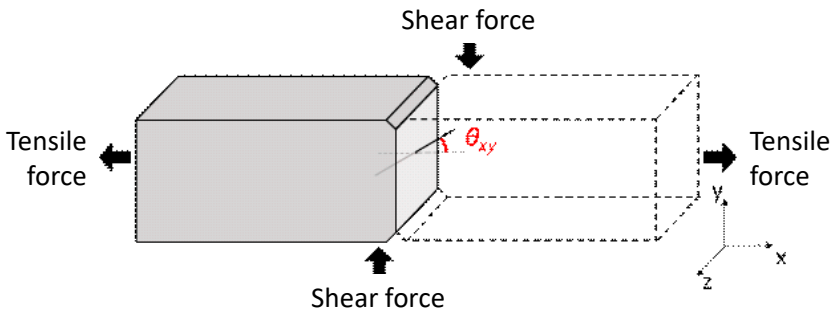

Fig. 4 – Definition of fiber orientation angle θ_{xy}

Table 2 shows the mixture proportion of FRCC and compression test results by 100 ϕ × 200mm cylinder test pieces. FRCC was prepared using high early strength portland cement with a water-cement ratio of 0.56 and 0.5% volume fraction of PVA fiber.

Table 2 – Mixture proportion of FRCC

Water-cement ratio (%)	Fiber volume fraction (%)	Unit weight (kg/m^3)					Compressive strength (MPa)	Elastic modulus (GPa)
		Water	Cement	Sand	Fly ash	PVA fiver		
0.56	0.5	380	678	484	291	6.5	47.0	17.2

2.2 Loading Method

Single plane shear tests under tensile load is conducted according to the loading method proposed in the previous study [1]. The loading method, measurement and loading history are shown in Fig. 5. The loading history of tensile and shear force simulates biaxial stress state of shear crack on FRCC structural members, where tensile force and shear force are simultaneously applied to the fibers and the shear deformation occurs after a certain amount of axial deformation. At first, only tensile force is applied by two oil jacks through the two screw bolts at both ends of the specimen. After the tensile force has been reached T_{max} = 7kN, the tensile force is reduce to the target tensile force T_c. Then, single plane shear loading is conducted under constant tensile force T_c. In the specimens of PP fiber on T_c = 0kN (T0), however, single plane shear test was conducted without applying tensile force. Deformations were measured by three pi-type LVDTs attached on both side of the specimens, and axial deformation w and shear deformation δ_s are calculated by the following equations. The symbols in the equations correspond to Fig. 5.

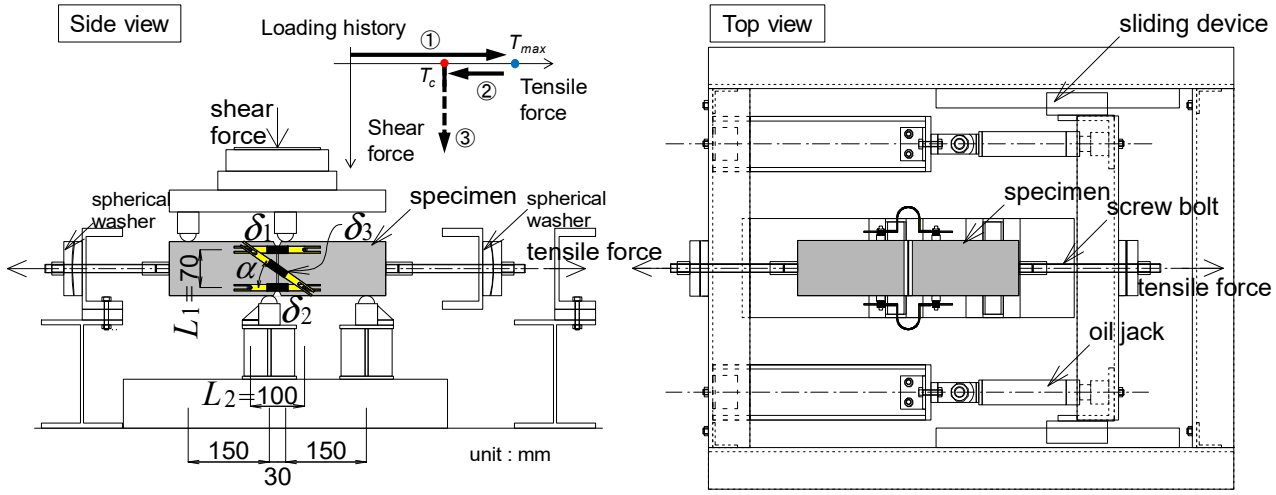

Fig. 5 – Loading system for single plane shear test

$$\delta_3 = \delta_s \cdot \sin\alpha + w \cdot \cos\alpha \tag{1}$$

$$w = \frac{(\delta_1 + \delta_2)}{2} \tag{2}$$

$$\delta_s = \delta_3 \cdot \frac{\sqrt{L_1^{\,2} + L_2^{\,2}}}{L_1} - \frac{\delta_1 + \delta_2}{2} \cdot \frac{L_2}{L_1} \tag{3}$$

3. Experimental Result

3.1 Failure patterns

Fig. 6 shows the examples of failure patterns after loading. The failure patterns are categorized in two types: failure by crack opening between the loading point and the tip of notch after increased shear deformation, and failure by crack opening at a position away from the assumed crack surface with the notch after increased shear deformation. In the former case, it is considered that crack opening occurred by shearing action around the assumed crack surface with pullout of fibers. In the latter case, it is considered that crack opening occurred by bending action with shear deformation of the assumed crack surface and the tensile force. The specimens under lower constant tensile force tend to fail by shear crack around the assumed crack surface. On the other hand, the specimens under higher constant tensile force tend to fail crack due to the bending action at a position away from the assumed crack.

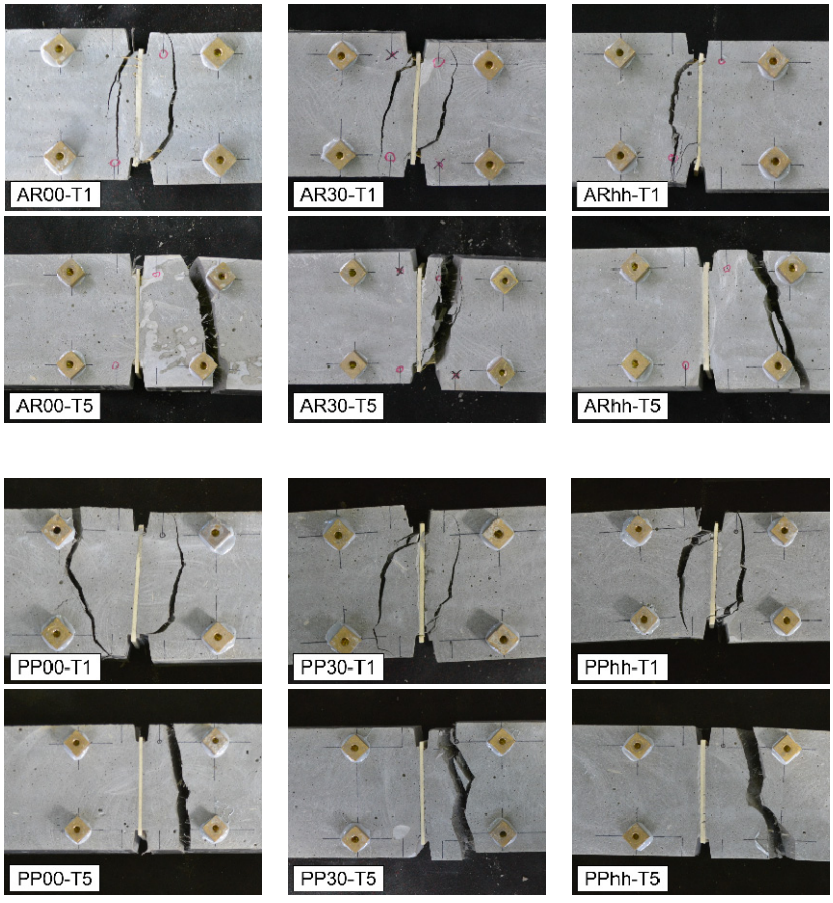

Fig. 6 – Failure patterns after loading

3.2 Load – Deformation relationships

Tensile load – axial deformation relationships, shear load – axial deformation relationships and shear load – shear deformation relationships of all specimens are shown in Fig. 7 to 12.

In AR00 specimens (aramid fiber orientation angle θ_{xy} = 0°), according to the tensile load – axial deformation relationships, the tensile stiffness tends to decrease from about tensile load 5kN during tensile loading up to the tensile force T_{max} = 7kN. According to the shear load – axial deformation relationships, the axial deformation increases after shear load reaches a maximum. According to the shear load – shear deformation relationships, the shear stiffness tends to decrease from about shear deformation 0.2mm. In addition, around the maximum shear load, the shear deformation increases with almost constant shear load. After that, shear load suddenly drops and fails due to the occurrence of cracks in the FRCC around the assumed crack surface.

In AR30 specimens (aramid fiber orientation angle θ_{xy} = 30°), according to the tensile load – axial deformation relationships, the tensile stiffness decreases and the axial deformation suddenly increases from about tensile load 4kN which is smaller than that of AR00 specimens. It is considered that because the fibers begin to pull out from the assumed crack surface and turn in the same direction as the tensile force, the axial deformation suddenly increases. According to the shear load – shear deformation relationships, the shear stiffness is clearly lower than that of AR00 specimens.

In ARhh specimens (aramid fiber orientation angle θ_{xy} = (0°, 30°)), according to the tensile – axial deformation relationships, the tensile stiffness tends to decrease from about tensile load 5kN which is about the same as AR00 specimens, and the tensile stiffness after that is almost in the middle of AR00 specimens and AR30 specimens. According to the shear load – shear deformation relationships, the shear stiffness reduces from the shear load 5kN which is smaller than that of AR00 specimens, and the shear deformation at which the shear force reaches a maximum is larger than that of AR00 specimens.

In PP fiber specimens, according to the tensile load – axial deformation relationships, the tensile stiffness is smaller than one of aramid fiber specimens, and the trend in fiber orientation angle is, on the whole, similar to aramid fiber specimens. It is considered that the reduction of tensile stiffness is due to the difference in fiber surface shape.

The whole trend of shear load – shear deformation relationships is similar to aramid fiber specimens. In PP00 specimens, according to the shear load – shear deformation relationships, the shear stiffness decreases at about shear load 4kN, and the shear load become constant from around shear deformation 1mm. In PP30 specimens, the shear stiffness is clearly lower than one of PP00 specimens, and the shear load become constant from around shear deformation 4mm. In PPhh specimens, the shear stiffness decreases at around shear load 2kN, and the shear load become constant from around shear deformation 1.8mm. In PP fiber specimen under constant tensile force T_c = 5.0kN (T5), the shear load is not constant after the maximum load and specimen fails because capacity for shear is small

3.2 Maximum shear load – tensile load relationships

Fig. 13 shows the relationships between the maximum shear load and constant tensile load at the maximum load. The experimental results are shown in table 3 and table 4. Shear load is revised to include P-δ effect due to axial tensile force. Despite the difference in fiber type and the fiber orientation angle, the maximum shear load tends to decrease as the constant tensile load increases. No significant difference is shown between the fiber type and the orientation angle. However, the PP fiber specimens under constant tensile load T_c = 1kN (T1) have lower maximum shear load than that of the PP fiber specimens under constant tensile load T_c = 3kN (T3) in any orientation angle.

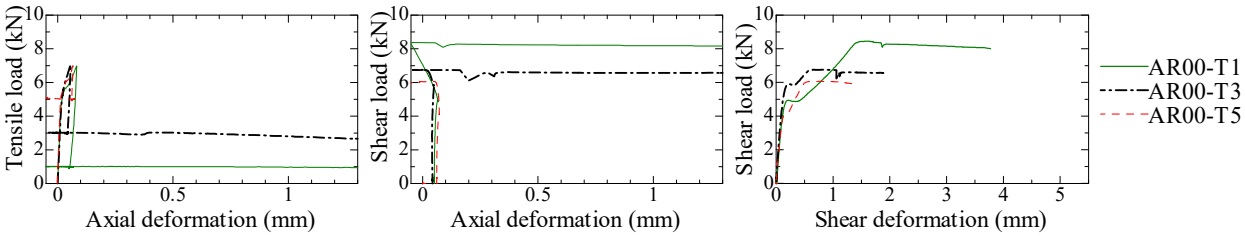

Fig. 7 – Relationship between tensile load, shear load, axial and shear deformation for AR00 specimen

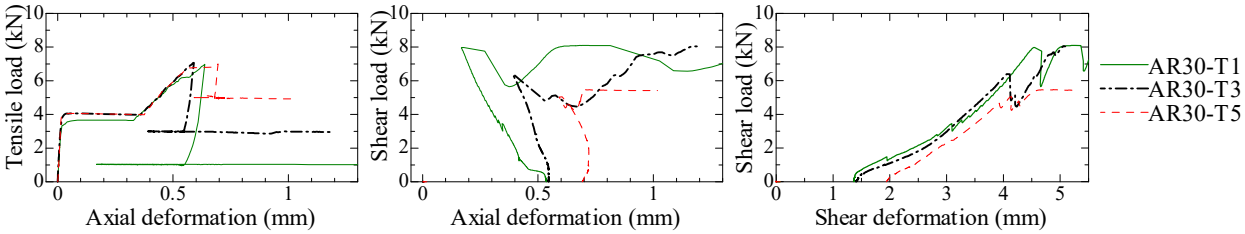

Fig. 8 – Relationship between tensile load, shear load, axial and shear deformation for AR30 specimen

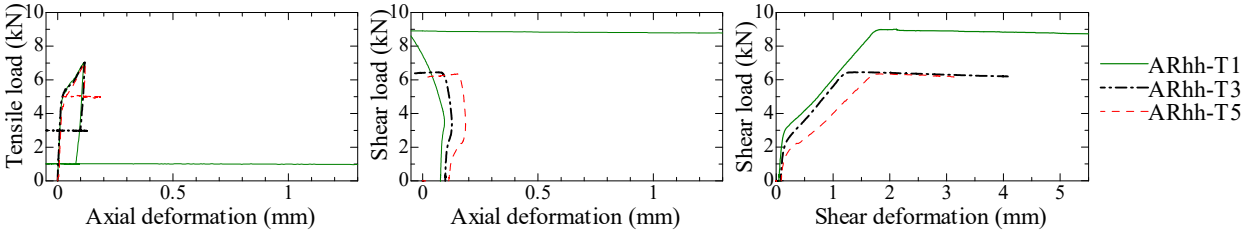

Fig. 9 – Relationship between tensile load, shear load, axial and shear deformation for ARhh specimen

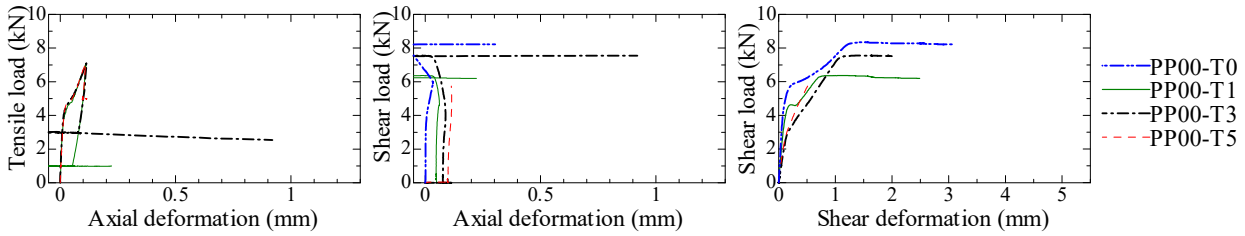

Fig. 10 – Relationship between tensile load, shear load, axial and shear deformation for PP00 specimen

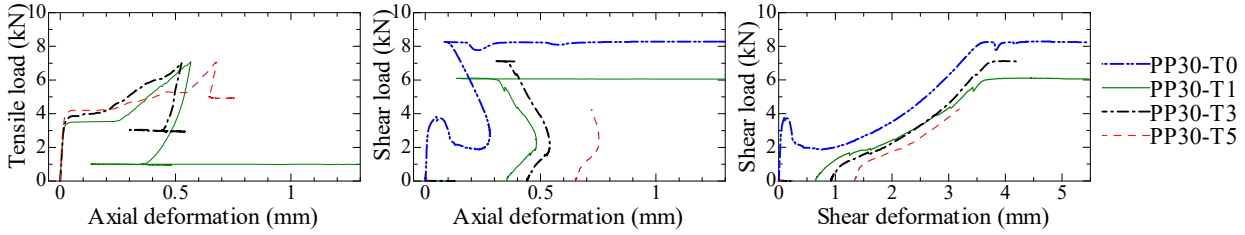

Fig. 11 – Relationship between tensile load, shear load, axial and shear deformation for PP30 specimen

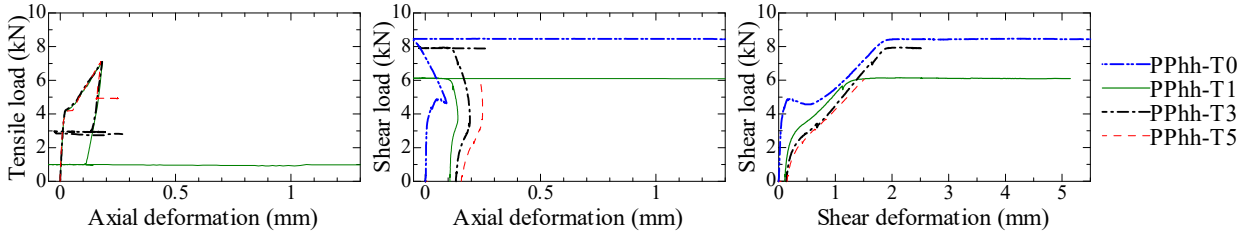

Fig. 12 – Relationship between tensile load, shear load, axial and shear deformation for PPhh specimen

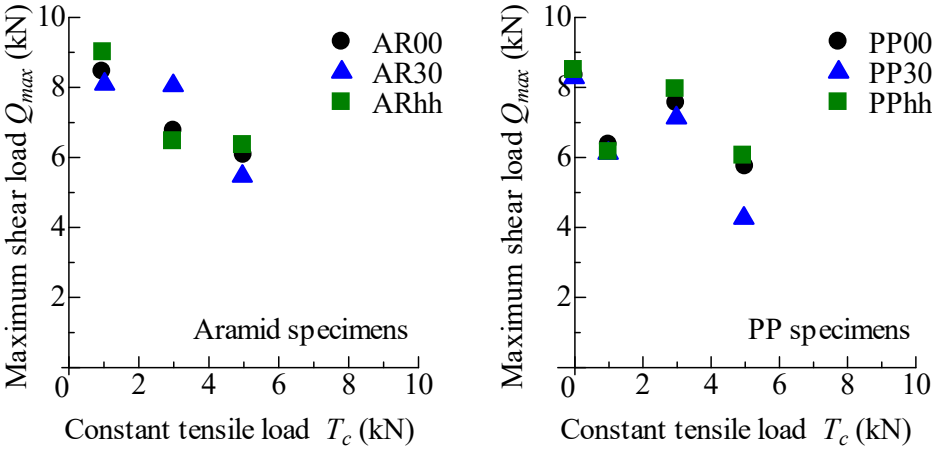

Fig. 13 – Maximum shear load – constant tensile load relationship

Table 3 – Experimental results of aramid specimens

Specimen ID	Fiber orientation angle [number of fibers]	Maximum tensile load (kN)	Constant tensile load (kN)	Maximum shear load (kN)
AR00-T1	0° [196]	6.98	0.96	8.45
AR00-T3		7.06	3.00	6.76
AR00-T5		7.00	5.00	6.07
AR30-T1	30° [196]	6.98	1.02	8.10
AR30-T3		7.06	2.98	8.05
AR30-T5		7.00	4.96	5.47
ARhh-T1	0° [98] 30°[98]	7.02	0.98	9.00
ARhh-T3		7.04	2.98	6.46
ARhh-T5		7.02	4.98	6.35

Table 4 – Experimental results of PP specimens

Specimen ID	Fiber orientation angle [number of fibers]	Maximum tensile load (kN)	Constant tensile load (kN)	Maximum shear load (kN)
PP00-T0	0° [196]	0	0	8.34
PP00-T1		7.08	1.00	6.37
PP00-T3		7.10	2.96	7.56
PP00-T5		7.08	4.98	5.74
PP30-T0	30° [196]	0	0	8.28
PP30-T1		7.08	1.00	6.12
PP30-T3		7.02	3.02	7.13
PP30-T5		7.08	4.96	4.27
PPhh-T0	0° [98] 30°[98]	0	0	8.49
PPhh-T1		7.10	1.00	6.15
PPhh-T3		7.10	2.94	7.95
PPhh-T5		7.12	4.94	6.05

4. Investigate of Shear Characteristics Using Fiber Bridging Law

According to the experimental results, normalized maximum shear force – tensile force relationships are shown in Fig. 14. Both maximum shear force and tensile force are normalized by maximum uniaxial tensile load P_a calculated by Eq. (4) [2]. For any fiber type and fiber orientation angle, the normalized maximum shear force tends to decrease linearly with increasing normalized tensile force. In order to quantify the decrease rate of the maximum shear force, the results of linear regression using a straight line passing through the maximum uniaxial tensile force are also shown in Fig. 14. The maximum shear stress of the fiber at the cracked surface is 0.33 times the uniaxial tensile strength for the aramid fiber and 0.34 times for the PP fiber.

$$P_a = P_{a,0} \cdot e^{f \cdot \theta} \cdot N \tag{4}$$

$$P_{a,0} = A \cdot l_b^{\,B} \tag{5}$$

Where,

$P_{a,0}$: Maximum pullout load of single fiber at 0 degrees orientation angle

l_b : Bond length

A, B : Coefficient by fiber type

Aramid fiber : $A = 26$, $B = 0.63$

PP fiber : $A = 25$, $B = 0.61$

N : Number of fibers at crack surface

f : Snubbing coefficient

Aramid fiber : $f = 0.083$

PP fiber : $f = 0.21$

θ : Fiber orientation angle

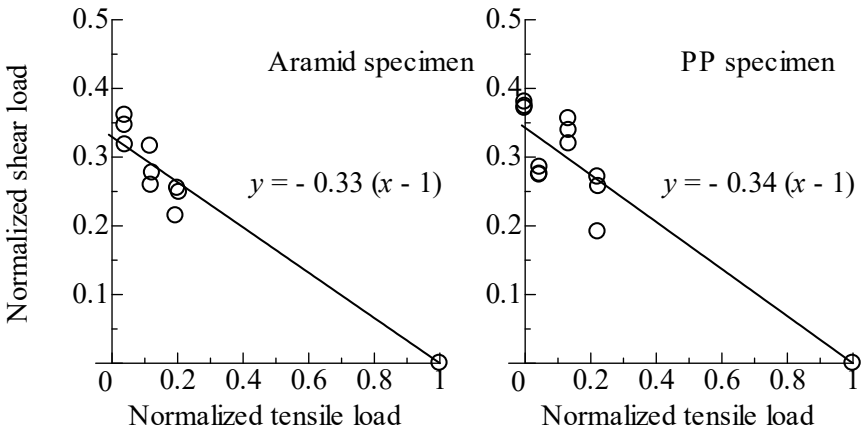

Fig. 14 – Normalized maximum shear load –constant tensile load relationship

5. Conclusions

To clarify shear bridging characteristics of aramid fibers and PP fibers on multiple stress condition of FRCC, single plane shear tests under tensile load are conducted. From the test results, the shear stiffness was confirmed to differ depending on the fiber type and fiber orientation angle. The shear deformation increased with alomost constant shear force after the maximum shear load. In the case of lower tensile force than uniaxial tensile strength, the shear strength of aramid and PP fiber decreased linearly by increase of the tensile force. The maximum shear stress of fibers under biaxial stress state was about one-third of uniaxial tensile strength calculated by bridging law despite the difference of the fiber type and fiber orientation angle.

6. Acknowledgements

This study was supported by JSPS KAKENHI Grant Number 18H03802.

7. References

[1] Kanakubo T., Shimizu K., Nagai S., Kanda T. (2010): Shear Transmission on Crack Surface of ECC. *7th International Conference on Fracture Mechanics of Concrete and Concrete Structures*, Vol.3, 1623-1630, Korea.

[2] Hashimoto H., Mu Y., Yamada H., Kanakubo T. (2017): Slip-Out Characteristics of Aramid and PP Fibers and Calculation of Bridging Law. *Concrete Research and Technology*, Vol.28, 103-111, Japan.

